

Image-Object-Specific Prompt Learning for Few-Shot Class-Incremental Learning

In-Ug Yoon
KAIST

iuyoon@rit.kaist.ac.kr

Tae-Min Choi
KAIST

tmchoi@rit.kaist.ac.kr

Sun-Kyung Lee
KAIST

sklee@rit.kaist.ac.kr

Young-Min Kim
Samsung Research

ym1012.kim@samsung.com

Jong-Hwan Kim
KAIST

jhkim@rit.kaist.ac.kr

Abstract

While numerous studies in few-shot class-incremental learning (FSCIL) have been conducted, attaining satisfactory performance, particularly during incremental sessions, remains a significant challenge. A key issue is that encoders, trained on extensive base session datasets, tend to underperform in subsequent incremental sessions. In this context, the Contrastive Language-Image Pre-training (CLIP) model, known for its ability to generalize to unseen classes, emerges as a promising option for FSCIL tasks. However, developing a learning scheme that effectively utilizes CLIP for FSCIL can be challenging, even showing a lower score in the final session than zero-shot learning. This is due to issues such as forgetting previous knowledge and insufficient learning ability for new sessions. We introduce a novel training framework centered around developing image-object-specific (IOS) classifiers to address the issues. Here, an IOS classifier is designed to focus on class objects' particular attributes (e.g., wings or wheels). Our framework is designed from an FSCIL perspective to maintain previously acquired knowledge and quickly adapt to new sessions without forgetting or overfitting. Our method consistently outperforms existing state-of-the-art techniques across datasets such as miniImageNet, CIFAR100, and CUB200. Also, we conduct further experiments to confirm the efficacy of our model in generating IOS classifiers and undertake ablation studies to evaluate the contribution of each component within our architecture.

1. Introduction

Class-Incremental Learning (CIL) is a deep learning algorithmic scheme designed to adapt quickly and efficiently to changes in the environment, while maintaining high perfor-

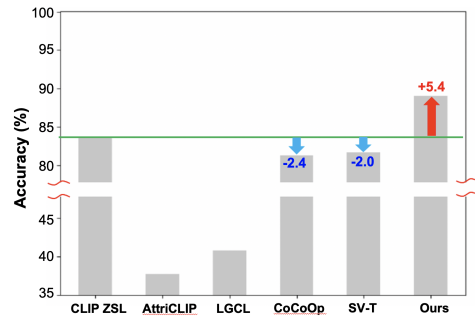


Figure 1. Comparison of various methods employing the CLIP model in terms of classification performance on all seen classes at the final session under the FSCIL setting. The results from CLIP zero-shot learning (ZSL) are remarkably impressive. However, other methods resulted in performance even lower than the CLIP ZSL outcomes. More detailed information on this experiment can be found in our supplementary materials.

mance. CIL is composed of sequential tasks, and for each task, only the training data from the current task should be accessible, to account for issues related to memory storage and data security. However, conventional CIL presupposes a substantial amount of training data for incremental sessions [10, 12, 21, 26], which can be challenging and time-consuming to obtain. Furthermore, the acquisition of such a dataset can impede the ability to swiftly adapt to changes. By comparison, humans can quickly adjust to new environments with only a limited number of training examples, without forgetting previous knowledge. Therefore, it is only logical to expect a deep learning algorithm that can adapt to new environments using just a few samples, without forgetting previous knowledge. This is precisely the goal of Few-Shot Class-Incremental Learning (FSCIL).

FSCIL comprises base and incremental sessions. An ample amount of training data is provided in the base session, while the classes in the incremental sessions are given only

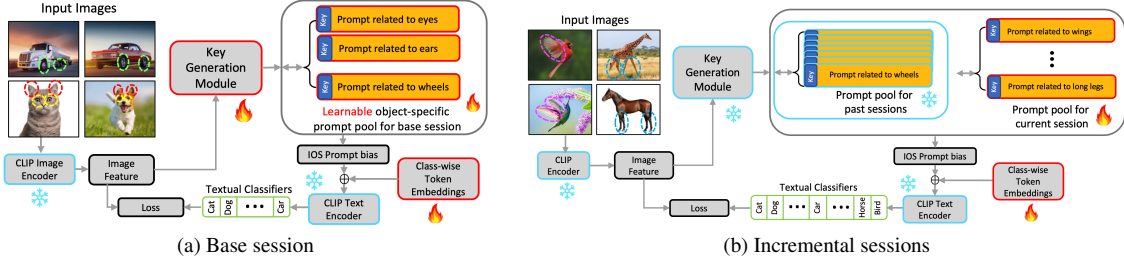


Figure 2. Conceptual illustration of our proposed training architecture for FSCIL. Our central idea revolves around generating and utilizing textual classifiers that encode the image-object-specific characteristics, harnessed using key-prompt pairs for each session. Icons with a fire symbol indicate learnable modules, while those with a freeze symbol represent frozen parameters.

a limited amount of training data. The primary challenge of FSCIL, similar to CIL, is to minimize forgetting of past sessions and prevent overfitting to the current session during the incremental learning process. Various strategies have been employed to tackle FSCIL, including the use of knowledge distillation [3, 5], pre-training of the feature extractor [2], and knowledge replay [13].

However, previous FSCIL methods have displayed clear limitations in their performance, particularly with regards to the classes in the incremental sessions. The underlying reason is as follows: Fine-tuning the substantial image encoder with a small quantity of training data in incremental sessions led to severe forgetting. In response, prior approaches either froze the model or incorporated simple networks for training [28, 29]. As a result, performance became largely dependent on the efficacy of the pre-trained image encoder in extracting features for new classes. However, image encoders have been trained on the base training dataset, which leads to significantly lower performance for new classes as compared to base session classes [3, 22, 28]. Therefore, a pre-trained model that exhibits high generalizability and is capable of extracting effective features from both seen and unseen class images, is needed to achieve superior performance in FSCIL tasks.

Recent research leveraging Contrastive Language-Image Pre-trained (CLIP) models has gained significant momentum, mainly due to their versatility, anchored in their paired image and text encoders. These models have also demonstrated their broad applicability, achieving notable results even in zero-shot classification tasks [17]. In Fig. 1, we examine the FSCIL performance of various CLIP-based methodologies. This includes applications in CIL (e.g., AttriCLIP [25] and LGCL [10]), generalization to unseen classes (e.g., CoCoOp [32]), and approaches for FSCIL (e.g., SV-T [16]). Our observations reveal that methods involving additional training exhibit a significant decline in performance as sessions progress, with final session outcomes occasionally falling below the zero-shot learning capabilities of CLIP. This decline is likely attributable to severe forgetting of past session knowledge and insufficient

learning for the new session during incremental session training. Moreover, strategies intended to mitigate these issues during incremental session training [10, 25], assuming ample training data for these sessions, have shown limited effectiveness in learning new tasks in FSCIL settings.

In this paper, addressing these challenges, we aim to develop an novel approach for FSCIL that capitalizes on the strengths of the CLIP model while circumventing the problems of forgetting and overfitting. We specifically focus on designing the learning structure to leverage image-object-specific (IOS) features and classifiers. The aspects of the learning structure, as illustrated in Fig. 2, are as follows:

Firstly, we propose a learning structure designed to capture the inherent IOS features from the image and incorporate them to the generated classifiers, which we term as IOS classifiers. Image features obtained by the CLIP image encoder have a formidable amount of information, including class object-related (which we refer as IOS), background-related, and more. However, for the classification, IOS characteristics (e.g., wings or wheels) plays the key role. Thus, we expected that focusing on the IOS characteristics could enhance both accuracy and efficiency for the classification.

Secondly, our learning scheme is designed to enhance the capability to acquire knowledge in incremental sessions with limited training data. Previously learned IOS characteristics may facilitate learning new classes that share similar attributes. Additionally, to support the acquisition of new IOS characteristics for the new session, we propose an initialization strategy to address the convergence issues that occur when proceeding with random initialization with only a few training data.

Finally, we tailored the learning scheme to minimize forgetting and overfitting during the incremental sessions. Specifically, we have carefully designed the update targets for the training phase of these sessions to prevent overfitting to the current session and forgetting past knowledge. In short, our contributions are as follows:

- We propose an image-object-specific prompt generation module to utilize object-related information within images when generating textual classifiers.

- Our learning scheme is designed to enhance the capability of learning new tasks, achieved via modules that capture IOS characteristics and a proposed initialization strategy to address convergence issues.
- We propose an optimized learning strategy to utilize the IOS classifiers for FSCIL, with perspective of minimizing the forgetting and overfitting issues during the incremental sessions.

2. Related Work

Few-shot class-incremental learning. The most challenging aspect of FSCIL is assimilating new knowledge for novel tasks without causing the forgetting of previously acquired knowledge. First line of approaches attempted to minimize the forgetting. The primary research objective in this area is to devise strategies to tackle this problem of forgetfulness.

One proposed solution entails employing neural gas to maintain the feature topology between the classes of the base and new sessions [22]. Another method involves data replay [13], where a certain amount of prior task data is stored in exemplar sets and utilized for replay during incremental sessions. Also, the technique of knowledge distillation has been applied, utilizing the model from earlier sessions as a guiding teacher model to mitigate forgetting [5].

Other approaches focus on the pre-training method during the base session to prepare for the upcoming incremental sessions. Meta-learning approaches aim to enhance the network’s adaptability to new tasks by creating episodic scenarios using base session data [8, 30]. Strategies that preserve regions of the embedding space for upcoming classes have also demonstrated performance improvements [29]. From the classifier’s perspective, an attention model was trained in the base session to balance the classifiers between past and new sessions during the incremental sessions [28]. However, despite these diverse attempts, the overall performance generally fell short of expectations, particularly for the incremental sessions.

Prompt Learning on CLIP Models for Continual Learning. Multi-modal large-scale models such as CLIP models recently showed remarkable usability, including the model generalizability for unseen classes, as shown in the zero-shot classification performance. To preserve the model expandability, researches added and updated the learnable prompts. Initial researches split dataset into base and new classes to evaluate. One line of work attempted to add prompts within the image and text encoders to reflect the learned knowledges [14]. Also replacing the basic text prompt to learnable prompts enhanced image classification performance [33]. Moreover, adding an image-specific prompt bias, prompt formed from image feature, to the learnable text prompts to form the textual classifiers en-

hanced the model performance on both seen and unseen classes [32]. Focusing on extracting object-specific information from the image to form the prompt bias also showed significant performance [7].

There were also approaches to utilize the CLIP model for class-incremental tasks. Learning task-wise attribute prompts for each task were proceeded, encoding both object-related and background-related attributes to form textual classifiers [25]. Learning both task-level and class-level guidance prompt for the sequential tasks verified the effectiveness [10]. Also aggregated structure of the image and textual features using the attention model was designed to form textual classifiers [31].

However, these methods were designed to train in incremental sessions based on a large number of current session training datasets and exemplar sets. Consequently, research has been carried out to utilize the CLIP model in FSCIL settings, which only have a few training data for incremental sessions. Such works have either added an average pooling and MLP layer to the pre-trained image transformer [16], or adapted learnable parameters to both the image and text encoders for each task [4].

3. Problem Set-up

FSCIL consists of sequential tasks having datasets $\mathcal{D} = \{\mathcal{D}^1, \mathcal{D}^2, \dots, \mathcal{D}^T\}$, where $\mathcal{D}^t = \{\mathcal{D}_{tr}^t, \mathcal{D}_{te}^t\}$ denotes training and test dataset for session t . Training set of session t , \mathcal{D}_{tr}^t consists of class labels $\mathcal{Y}_{tr}^t = \mathcal{Y}^t = \{y_1^t, \dots, y_{m^t}^t\}$, where m^t is the number of classes in session t . Note that different sessions have no overlapped classes, *i.e.* $\forall i, j$ and $i \neq j$, $\mathcal{Y}^i \cap \mathcal{Y}^j = \emptyset$. Test set of session t , \mathcal{D}_{te}^t is composed of class labels $\mathcal{Y}^1 \cup \mathcal{Y}^2 \dots \cup \mathcal{Y}^t$. For convenience, we denote $\mathcal{Y}^{i:j} = \mathcal{Y}^i \cup \dots \cup \mathcal{Y}^j$ for $i < j$. For N -way K -shot FSCIL setting, $|\mathcal{D}_{tr}^t| = K \times N$, $m^t = N$ for $t > 1$.

CLIP image encoder and text encoder are denoted as $f_I(\cdot) \in \mathbb{R}^D$ and $f_T(\cdot) \in \mathbb{R}^D$, where D is the embedded dimension. With the text input x_{text} and length function $L(x_{text})$ which outputs the length of the tokenized input text, the CLIP tokenized embedding function is denoted as $h(x_{text}) \in \mathbb{R}^{L(x_{text}) \times D}$.

4. Method

In this section, we introduce the overall training procedures which are illustrated in Fig. 3. The following steps are proceeded for each session. Note the commonalities and differences between base and incremental sessions for each step. We use session index $t \in \{1, \dots, T\}$, where $t = 1$ denotes the base session and else denotes the incremental sessions.

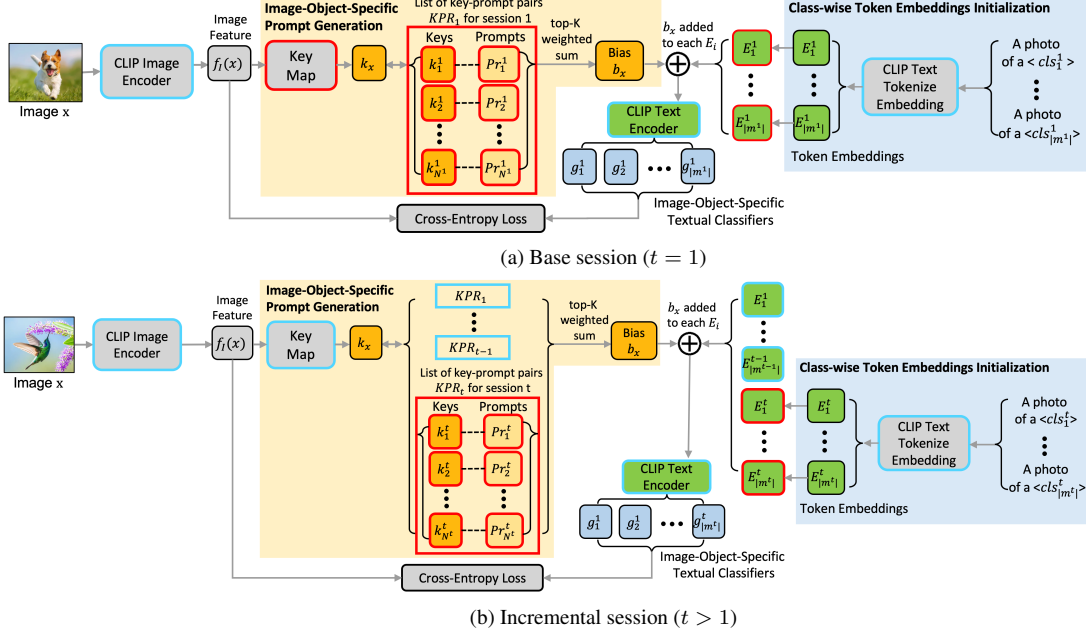


Figure 3. An overview of our training framework encompasses the ‘class-wise token embedding initialization’ and ‘image-object-specific prompt generation’ modules. We leverage these modules to capture the IOS attributes within images and reflect them to the generated classifiers. Note that we elaborately designed the updatability of each module in every session to mitigate forgetting, where a red borderline module indicates learnable while a blue borderline module indicates frozen.

4.1. Initialization of class-wise token embeddings

We utilize learnable class-wise token embeddings which is used to generate a textual classifier for each class. For the initialization of embeddings within the session t , we first consider the basic prompt $P_i^t = \text{‘a photo of a } [CLS]_i^t \text{’}$, where $[CLS]_i^t$ is a class name corresponding to the class label y_i^t for $i \in \{1, \dots, m^t\}$. Then the class-wise token embedding of each class is initialized as

$$E_i^t = h(P_i^t), \quad (1)$$

where $E_i^t \in \mathbb{R}^{L(P_i^t) \times D}$. Note that the length of encoded token for each class may differ in length, which is why we use length function $L(\cdot)$ to specify the dimension.

4.2. Image-object-specific prompt generation

To reflect the object-specific information within the image to the textual classifiers, we introduce an image-object-specific prompt generation module. With the input image and class label $(x, y) \in \mathcal{D}_{tr}^t$, we first obtain image feature as

$$f(x) = f_I(x), \quad (2)$$

Then we define the following key-map function to obtain a key incorporating information of image feature:

$$k_x = g_\theta(f(x)), \quad (3)$$

where $k_x \in \mathbb{R}^D$. Then we set the number of key-prompt pairs to catch the object-specific features within the session. For each session, we construct key-prompt pairs as $\{k_i^t, P_{r_i}^t\}_{i=1}^{N^t}$, where N^t is the number of key-prompt pairs used for session t . To create image-object-specific prompts, as each image can possess multiple object-related attributes, we calculate the similarities between k_x and keys and then merge prompts associated with keys exhibiting significant similarities. We calculate the similarities between the provided k_x and keys, then select indices with notable similarities using the following two-dimensional $top-K$ function with $K = K_{pr}$, as elucidated in our supplementary materials:

$$\{t_j, h_j\}_{j=1}^{K_{pr}} = \arg \text{top-K} \{ \{ \text{sim}(k_x, k_i^{t'}) \}_{i=1}^{N^{t'}} \}_{t'=1}^t, \quad (4)$$

where $\text{sim}(\cdot, \cdot)$ is a cosine similarity function and K_{pr} is number of prompts combined for bias. Note that we compare the k_x with the keys, including the past sessions, since the class of a new session might have an object features from the past sessions. To combine the prompts corresponding to keys with high similarity, we achieve the weights as follows:

$$w_j = \frac{\exp(\text{sim}(k_x, k_{h_j}^{t_j}))}{\sum_{i=1}^{K_{pr}} \exp(\text{sim}(k_x, k_{h_i}^{t_i}))}, \quad (5)$$

for $j \in \{1, \dots, K_{pr}\}$ where $\exp(\cdot)$ is an exponention function. Note that a softmax function is employed to make the sum of weights to 1. Finally, the image-object-specific prompt is generated as follows:

$$b_x = \sum_{j=1}^{K_{pr}} w_j * Pr_{h_j}^{t_j}. \quad (6)$$

4.3. Initialization of key-prompt pairs

In this section, we introduce our initialization method for key-prompt pairs. Through empirical observation, we identified that training the parameters initialized randomly only with few samples during the incremental sessions leads to challenges in updating the model to a convergence point with satisfactory performance. Thus we search for the initialization method instead of using random values. Given our aim to capture the inherent objective features within each class through key-prompt pairs, it is anticipated that leveraging class-wise token embeddings would likely result in successful convergence. So given N^t as the number of key-prompt pairs used for session $t \in \{1, \dots, T\}$, we initialized the key-prompt pair as

$$k_i^t = f_T(E_j^t), Pr_i^t = E_j^t, \quad (7)$$

where $i \in \{1, \dots, N^t\}$ denotes the index for a pair and $j \in \{1, \dots, m^t\}$ is a randomly chosen class index from the session t . As demonstrated through our experiments, our initialization method exhibits exceptional performance. Additionally, we observed that the random selection of indices did not significantly influence the outcomes, as shown with further ablation studies in our supplementary materials. This is attributed to the crucial aspect of initializing vectors within the prompt space formed by the text encoders instead of the entire embedded space. The primary factor impacting overall performance was the number of pairs N^t . Note that we also applied the proposed key-prompt initialization method for the base session with ample training set since the results were lower when they were randomly initialized, as shown in the experimental section.

4.4. Image-object-specific textual classifiers

With the class-wise token embeddings and generated image-object-specific bias b_x , we now generate the textual classifiers. Textual classifiers for each class is generated as

$$g_i^{t'} = f_T(b_x + E_i^{t'}), \quad (8)$$

for session index $t' \in \{1, \dots, t\}$ and class index $i \in \{1, \dots, m^{t'}\}$.

4.5. Training using the loss function

After achieving the textual classifiers, we now calculate the loss function to update the model. We first calculate logits

for all currently seen classes. For each image $(x, y) \in \mathcal{D}_{tr}^t$ and session index $t' \in \{1, \dots, t\}$, the probability logit for each class is calculated using softmax function as

$$p(y_i^{t'} | x) = \frac{\exp(\text{sim}(f(x), g_i^{t'}))}{\sum_{t'=1}^t \sum_{j=1}^{m^{t'}} \exp(\text{sim}(f(x), g_j^{t'}))}, \quad (9)$$

for class index $i \in \{1, \dots, m^{t'}\}$. Next, we employ the following cross-entropy function to compute the loss for the update:

$$\mathcal{L}_{CE}(x, y) = - \sum_{t'=1}^t \sum_{i=1}^{m^{t'}} \mathbb{1}[y_i^{t'} == y] \log(p(y_i^{t'} | x)), \quad (10)$$

where $\mathbb{1}(\cdot)$ is an indicator function. Finally, the model is updated via the calculated loss. We distinguish the explanations of base and incremental sessions to emphasize the difference in training.

Base session. In the base session, based on the sufficient amount of training data and relatively large number of classes, the key-map network is trained to extract effective key from the image to compare with the key-prompt pairs, resulting to form IOS bias for the text classifier generation. Also, the network modules corresponding to the base session are updated (e.g. key-prompt pair and class-wise token embedding). The model is updated to optimize the following equation:

$$\min_{\theta, E^1, k^1, Pr^1} \mathbb{E}_{(x,y) \sim \mathcal{D}_{tr}^1} [\mathcal{L}_{CE}(x, y)], \quad (11)$$

where θ is from Eq. 3. E^1 , k^1 and Pr^1 denote $\{E_i^1\}_{i=1}^{m^1}$, $\{k_i^1\}_{i=1}^{m^1}$, and $\{Pr_i^1\}_{i=1}^{m^1}$, respectively.

Incremental sessions. The challenge of training during incremental sessions stems from the lack of training data for past sessions, resulting in severe overfitting with high scores for the new session but poor performance on previous ones. Conversely, efforts to minimize network updates to preserve performance on past sessions have not yielded satisfactory results for new sessions [27–29]. To address these issues, we meticulously designed the update targets during incremental session training. This approach involves updating only the network modules pertinent to the current session, as detailed in the following equation:

$$\min_{E^t, k^t, Pr^t} \mathbb{E}_{(x,y) \sim \mathcal{D}_{tr}^t} [\mathcal{L}_{CE}(x, y)], \quad (12)$$

where E^t , k^t and Pr^t denote $\{E_i^t\}_{i=1}^{m^t}$, $\{k_i^t\}_{i=1}^{m^t}$, and $\{Pr_i^t\}_{i=1}^{m^t}$, respectively. Note that we exclusively update the parameters of the current session to retain knowledge from previous sessions and minimize forgetting.

Method	Backbone	Acc. in each session \uparrow (%)									AVG(\uparrow)	PD(\downarrow)
		1	2	3	4	5	6	7	8	9		
FACT[29]	ResNet18	72.6	69.6	66.4	62.8	60.6	57.3	54.3	52.2	50.5	60.7	22.1
ALICE [15]	ResNet18	80.6	70.6	67.4	64.5	62.5	60.0	57.8	56.8	55.7	64.0	24.9
BSC [27]	ResNet18	78.4	74.6	71.4	68.7	65.9	63.6	62.0	60.3	58.5	67.1	19.8
ALICE [15]*	ViT-B	85.7	77.3	73.1	71.5	68.9	65.1	62.3	59.9	58.1	69.4	30.6
BSC [27]*	ViT-B	85.2	80.4	76.4	73.2	70.0	67.2	64.5	62.7	61.5	71.6	26.7
CLIP ZSL*	ViT-B/16	85.8	85.5	84.9	84.8	84.2	84.2	84.0	83.9	83.7	84.6	2.1
SV-T [16]	ViT-B/16	90.6	89.2	86.8	85.4	84.8	83.4	81.9	81.9	81.7	85.1	8.9
CoCoOp [32]*	ViT-B/16	94.2	91.7	88.9	87.8	86.3	84.3	82.5	81.9	81.3	86.5	12.9
Ours	ViT-B/16	95.4	94.4	93.4	93.1	92.1	91.4	90.8	90.0	89.1	92.2	6.3

Table 1. Comparison with state-of-the-art methods on the miniImageNet dataset in a 5-way 5-shot setting. \uparrow means higher is better, while \downarrow denotes lower is better. The double horizontal line distinguish whether the CLIP model was used. * mark denotes the re-implemented results, where we re-implemented the CLIP ZSL (zero-shot learning) and CoCoOp for the FSCIL task. Also, we re-implemented ALICE and BSC using ViT-B backbone. Note that we only included results that clearly specify the type of CLIP model used. Full comparison table is in our supplementary materials.

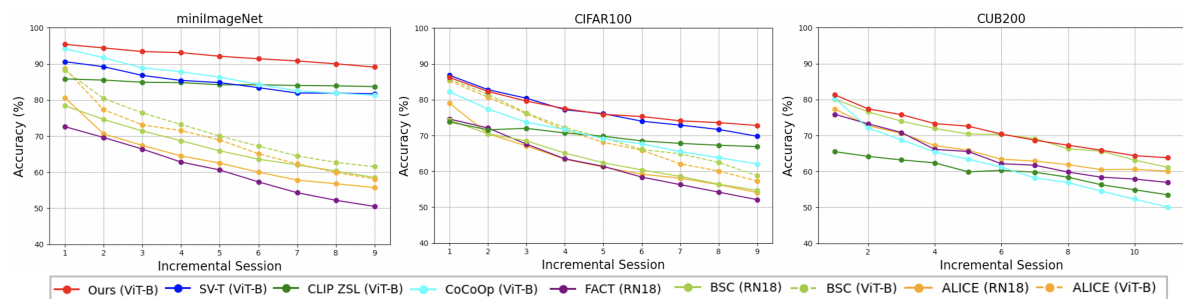


Figure 4. Comparison with the state-of-the-art methods on diverse datasets. Note that for the CUB200 dataset, the previous methods without using the CLIP model utilize ImageNet-pretrained model due to the difficulty of fine-grained dataset.

5. Experiments

5.1. Experimental Setup

Dataset. We conducted performance evaluations of the comparative methods across three widely-used datasets: miniImageNet [23], CUB200 [24], and CIFAR100 [11]. The miniImageNet dataset, a 100-class subset of ImageNet-1k [19], is commonly employed in few-shot learning. It contains 500 training images and 100 test images for each class, with each image measuring 84×84 pixels. CIFAR100 offers 100 classes, each containing 500 training images and 100 test images, with each image having dimensions of 32×32 pixels. The CUB200 dataset includes around 6,000 training images and 6,000 test images spread over 200 bird classes, having 224×224 pixel size.

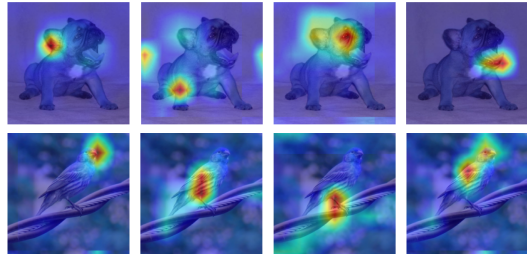
In line with the experimental design of previous work, we randomly chose 60 classes as base classes for miniImageNet and CIFAR100, dividing the remaining incremental classes into eight sessions, each encompassing five classes. For CUB200, we split the data into 100 base classes and 100 incremental classes, with the incremental classes fur-

ther divided into ten sessions of ten classes each. For all datasets, we used five training images for each class in our 5-shot experiments, and we utilized all test images to assess generalization performance and avoid overfitting.

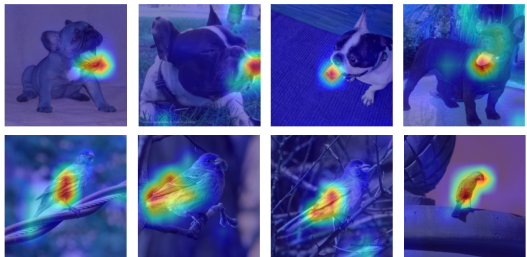
Evaluation protocol. Prior research primarily used the average accuracy (AVG) and performance dropping (PD) as the key metric to demonstrate the efficacy of the algorithms. AVG is the average performance over all sessions and PD is defined as the absolute difference in test accuracy between the base session and the final session. To elaborate, we denote $\mathcal{A}_{\mathcal{Y}}^t$ as the accuracy assessed solely on the test sets of classes \mathcal{Y} . Here, probabilities are calculated among classes $\mathcal{Y}^{1:t}$, using the network model trained after the t^{th} session. Then, AVG and PD are respectively defined as

$$AVG = \frac{\sum_{t=1}^T \mathcal{A}_{\mathcal{Y}^{1:t}}^t}{T}, \quad PD = \mathcal{A}_{\mathcal{Y}^1}^1 - \mathcal{A}_{\mathcal{Y}^{1:T}}^T. \quad (13)$$

To precisely measure the performance of the model during the sessions on classes of base and incremental sessions, we further use the following metrics [27] to measure the new task learning ability (NLA) and base task maintaining



(a) Role of different prompts of the same image



(b) Role of a single prompt on different images

Figure 5. Visualization of the role of the learned prompts.

ability (BMA):

$$NLA = \frac{\sum_{t=2}^T \mathcal{A}_{y^{2:t}}^t}{T-1}, \quad BMA = \frac{\sum_{t=1}^T \mathcal{A}_{y^1}^t}{T}. \quad (14)$$

Implementation details. In the experiments, we utilized the ViT-B/16 model [6] as the backbone for CLIP. We used 5 for base and 3 for incremental sessions as training epochs. Default top-K value used for key-prompt pair was 3, and the number used for key-prompt pairs were 20 and 3 for base and incremental sessions, respectively. Note that all values reported in this paper are average of results from 10 individual runs to reduce the randomness. Further details are described in our supplementary materials.

5.2. Main Results

Comparison with the state-of-the-art methods. We compared our proposed method with the state-of-the-art FS-CIL methods. Considering that the utilization of the CLIP model inherently results in improved performance, we distinguished between methods employing the CLIP model in Table 1. Additionally, since the CLIP model does not offer the commonly-used ResNet18 backbone found in previous methods, we chose to use the ViT-B backbone for CLIP. This led us to re-implement previous methods using the same backbone. As evidenced in Table 1 and Fig. 4, our method surpasses the state-of-the-art models on the CIFAR100, miniImageNet, and CUB200 datasets.

Visualization of the efficacy of image-object-specific modules. To validate our claim that our key-prompts are designed to capture image-object-specific features, we employ the attention map visualization method for transformer models [1]. To emphasize the characteristics of each

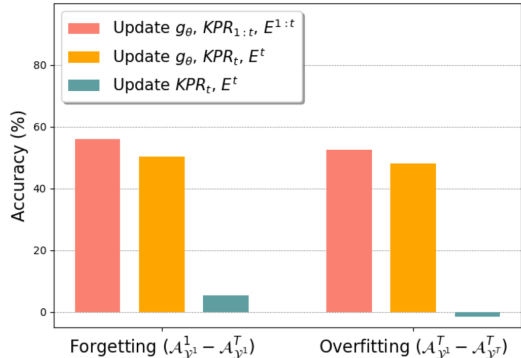


Figure 6. Effects of the parameter update range during incremental session training on forgetting and overfitting. The parameter notation follows from Fig. 3. To assess forgetting, we compare the base session performance of the model after the base session training with that after the final session. To evaluate overfitting, we compare the performance on both the base and final sessions after the final session training.

Loss	AVG(\uparrow)	PD(\downarrow)	NLA(\uparrow)	BMA(\uparrow)
CEC* [28]	57.7	24.6	18.6	68.3
FACT* [29]	60.7	22.1	13.5	75.2
BSC* [27]	68.7	20.2	37.8	77.8
CLIP ZSL*	84.6	2.1	85.5	84.2
CoCoOp*	86.5	12.9	86.1	86.9
Ours	92.2	6.3	91.1	92.4

Table 2. Comparison of methods on miniImageNet with additional metrics. * denotes the re-implemented results.

learned key-prompt pair, we display the image content that correlates with each prompt. To highlight the image content influencing the classification for each class, we compute the loss between the image feature and the generated textual classifiers. With the trained key-prompts using Eq. 6, we analyze the role of each prompt. In Fig. 5a, different columns correspond to distinct prompts from the selected $top-K$ prompts extracted from the given image. We could see that different prompts encapsulate diverse object attributes. To verify the functionality of each prompt, we apply a single prompt across diverse images, as shown in Fig. 5b. We observe that attention from the same prompt highlights similar object features. Moreover, we observed that the majority of these features are related to the objects themselves rather than the background.

Effectiveness on reducing the overfitting and the forgetting. During incremental session training, our learning scheme was tailored to minimize forgetting past session knowledge and overfitting to the new session. To examine the impact of our update scheme on overfitting and forgetting, we conducted an ablation study, as depicted in Fig. 6. The findings highlight the significance of the choice of parameters to be updated. Specifically, updating the key-

Method	Init.	cls-wise	Key map	Acc. in each session [†] (%)									AVG(\uparrow)	PD(\downarrow)	NLA(\uparrow)	BMA(\uparrow)
				1	2	3	4	5	6	7	8	9				
Ours (ViT-B/16)	✓	✗	FC1	91.3	85.2	81.3	76.2	73.4	68.4	62.3	59.3	56.2	72.6	35.1	57.3	76.2
Ours (ViT-B/16)	✗	✓	FC1	91.5	76.5	65.2	59.2	51.2	48.7	44.2	41.8	39.5	57.5	52.0	15.7	71.3
Ours (ViT-B/16)	Inc.	✓	FC1	91.5	90.2	89.5	89.1	88.3	87.7	86.9	85.8	84.9	88.2	6.6	86.3	89.8
Ours (ViT-B/16)	✓	✓	FC2	95.5	94.1	92.6	91.2	89.5	89.2	88.9	88.6	88.3	90.9	7.2	89.8	91.2
Ours (ViT-B/16)	✓	✓	RES2	95.5	94.2	93.1	92.1	91.1	90.3	89.9	88.8	88.6	91.5	6.9	90.3	91.8
Ours (ResNet101)	✓	✓	FC1	91.2	87.3	86.4	86.2	85.4	85.1	85.0	84.3	84.0	86.1	7.2	83.5	88.5
Ours (ViT-B/16)	✓	✓	FC1	95.4	94.4	93.4	93.1	92.1	91.4	90.8	90.0	89.1	92.2	6.3	91.1	92.4

Table 3. Ablation study of the proposed method on miniImageNet dataset in a 5-way 5-shot setting. ‘cls-wise’ specifies whether cls-wise token embedding was used, ‘Init.’ denotes whether the initialization trick was applied (‘Inc.’ means that the trick is applied only for incremental sessions), and ‘Key-map’ refers to the model type for the key map. FC1 and FC2 denotes the fully connected layer with one and two layers, while RES2 denotes FC2 with residual path added. The detailed structures are described in our supplementary materials.

N^1	$N^t(t > 1)$	AVG(\uparrow)	PD(\downarrow)	NLA(\uparrow)	BMA(\uparrow)
20	1	91.9	6.7	90.2	92.1
20	3	92.2	6.3	91.1	92.4
40	3	92.1	6.4	90.8	92.2
60	5	90.0	10.5	88.5	90.4
100	10	86.3	14.2	84.2	87.2

Table 4. Ablation study on the number of key-prompt pairs N^t for base and incremental sessions.

top-K	AVG(\uparrow)	PD(\downarrow)	NLA(\uparrow)	BMA(\uparrow)
1	91.8	6.7	90.3	92.0
2	92.0	6.5	90.8	92.3
3	92.2	6.3	91.1	92.4
4	92.1	6.4	90.7	92.4
5	91.3	7.5	90.0	91.5

Table 5. Ablation study on top-K value used for prompt bias generation.

map network, which is utilized for both base and incremental classes, solely with current session training data led to substantial forgetting and overfitting. In contrast, updating only the parameters related to the current session yielded the most favorable results.

Furthermore, we compared our results on the NLA and BMA metrics, respectively representing the overall ability to learn new tasks and maintain knowledge of previous sessions without forgetting, with prior FSCIL works in Table 2. Our method demonstrates superb performance across all metrics, effectively reducing both forgetting and overfitting.

5.3. Ablation Studies

Effects of initialization methods. In the preceding sections, we utilized initialization tricks for key-prompt pairs with two objectives. Firstly, since the primary objective of key-prompt pairs is to capture class-specific object features, we anticipated that initializing with class-wise token embeddings would facilitate convergence. Secondly, considering the limited amount of training data available in incremental sessions, initializing parameters with meaningful

vector values instead of random ones could help alleviate potential issues of severe overfitting. As seen in Table 3 (row 2 vs. 7), using random initialization led to convergence failures in the incremental sessions. Our proposed initialization method significantly increased NLA (2 vs. 3), confirming its effectiveness for learning in incremental sessions. Additionally, (3 vs. 7) implies that applying random initialization to the base session results in a decrease in overall performance.

Using the classwise learnable token embeddings. In this paper, we used learnable token embeddings for each class, instead of using common learnable embedding as in [33]. The purpose of adopting class-wise embeddings is to enhance the model’s capacity to capture the unique features of each class. Using common embedding instead of class-wise results in catastrophic forgetting during the incremental sessions, as shown in Table 3 (1 vs. 7).

Network for key-map. Ablation study on the key-map network structure in Table 3 (4,5 vs. 7) shows that using FC2 and RES2 slightly reduced performances compared to FC1. We infer from the results that a single fully connected layer is sufficient for the key-map network structure, and larger models diminish performance.

Number of prompt-key pairs for each session. As shown in Table 4, changes in the number of key-prompt pairs resulted in slight changes to the performance. Note that using a number smaller than the total class number led to better score, which may be due to the inclusion of shared features among similar classes enhancing the performance.

Number of the top-K values. We further proceeded to analyze the effect of the number of $top - K$ value used in Eq. 4 to the overall performance. As we can see from Table 5, using less or too much matched prompts to combine the prompt bias decreased the performance.

6. Conclusion

In this paper, we proposed a training architecture for the FSCIL task using image-object-specific (IOS) textual clas-

sifiers, generated through our proposed IOS prompt bias generation module. Concerning the generation module, we crafted the architecture to reduce past knowledge forgetting and current session overfitting during incremental session training. Our method demonstrated marked enhancements compared to state-of-the-art approaches, and we confirmed the presence of IOS features in the generated classifiers. Furthermore, we offer ablation studies to analyze the effects of each module used within the training architecture.

References

- [1] Hila Chefer, Shir Gur, and Lior Wolf. Generic attention-model explainability for interpreting bi-modal and encoder-decoder transformers. In *Proceedings of the IEEE/CVF International Conference on Computer Vision*, pages 397–406, 2021. [7](#)
- [2] Kuilin Chen and Chi-Guhn Lee. Incremental few-shot learning via vector quantization in deep embedded space. In *International Conference on Learning Representations*, 2020. [2](#), [12](#), [13](#)
- [3] Ali Cheraghian, Shafin Rahman, Pengfei Fang, Soumava Kumar Roy, Lars Petersson, and Mehrtash Harandi. Semantic-aware knowledge distillation for few-shot class-incremental learning. In *Proceedings of the IEEE/CVF Conference on Computer Vision and Pattern Recognition*, pages 2534–2543, 2021. [2](#), [13](#)
- [4] Marco D’Alessandro, Alberto Alonso, Enrique Calabrés, and Mikel Galar. Multimodal parameter-efficient few-shot class incremental learning. *arXiv preprint arXiv:2303.04751*, 2023. [3](#)
- [5] Songlin Dong, Xiaopeng Hong, Xiaoyu Tao, Xinyuan Chang, Xing Wei, and Yihong Gong. Few-shot class-incremental learning via relation knowledge distillation. In *Proceedings of the AAAI Conference on Artificial Intelligence*, pages 1255–1263, 2021. [2](#), [3](#), [13](#)
- [6] Alexey Dosovitskiy, Lucas Beyer, Alexander Kolesnikov, Dirk Weissenborn, Xiaohua Zhai, Thomas Unterthiner, Mostafa Dehghani, Matthias Minderer, Georg Heigold, Sylvain Gelly, et al. An image is worth 16x16 words: Transformers for image recognition at scale. *arXiv preprint arXiv:2010.11929*, 2020. [7](#)
- [7] Koustava Goswami, Srikrishna Karanam, Prateksha Udhayan, Balaji Vasani Srinivasan, et al. Contextual prompt learning for vision-language understanding. *arXiv preprint arXiv:2307.00910*, 2023. [3](#)
- [8] Michael Hersche, Geethan Karunaratne, Giovanni Cherubini, Luca Benini, Abu Sebastian, and Abbas Rahimi. Constrained few-shot class-incremental learning. In *Proceedings of the IEEE/CVF Conference on Computer Vision and Pattern Recognition*, pages 9057–9067, 2022. [3](#), [12](#), [13](#)
- [9] Zhong Ji, Zhishen Hou, Xiyao Liu, Yanwei Pang, and Xuelong Li. Memorizing complementation network for few-shot class-incremental learning. *arXiv preprint arXiv:2208.05610*, 2022. [12](#), [13](#)
- [10] Muhammad Gul Zain Ali Khan, Muhammad Ferjad Naem, Luc Van Gool, Didier Stricker, Federico Tombari, and Muhammad Zeshan Afzal. Introducing language guidance in prompt-based continual learning. In *Proceedings of the IEEE/CVF International Conference on Computer Vision*, pages 11463–11473, 2023. [1](#), [2](#), [3](#), [12](#)
- [11] Alex Krizhevsky, Vinod Nair, and Geoffrey Hinton. Cifar-10, cifar-100 (canadian institute for advanced research), 2019. [6](#)
- [12] Depeng Li, Tianqi Wang, Junwei Chen, Kenji Kawaguchi, Cheng Lian, and Zhigang Zeng. Multi-view class incremental learning. *arXiv preprint arXiv:2306.09675*, 2023. [1](#)
- [13] Huan Liu, Li Gu, Zhixiang Chi, Yang Wang, Yuanhao Yu, Jun Chen, and Jin Tang. Few-shot class-incremental learning via entropy-regularized data-free replay. *arXiv preprint arXiv:2207.11213*, 2022. [2](#), [3](#), [12](#), [13](#)
- [14] Yongzhu Miao, Shasha Li, Jintao Tang, and Ting Wang. Mudpt: Multi-modal deep-symphysis prompt tuning for large pre-trained vision-language models. *arXiv preprint arXiv:2306.11400*, 2023. [3](#)
- [15] Can Peng, Kun Zhao, Tianren Wang, Meng Li, and Brian C Lovell. Few-shot class-incremental learning from an open-set perspective. In *European Conference on Computer Vision*, pages 382–397. Springer, 2022. [6](#), [12](#), [13](#)
- [16] Wenhao Qiu, Sichao Fu, Jingyi Zhang, Chengxiang Lei, and Qinnu Peng. Semantic-visual guided transformer for few-shot class-incremental learning. *arXiv preprint arXiv:2303.15494*, 2023. [2](#), [3](#), [6](#), [12](#), [13](#)
- [17] Alec Radford, Jong Wook Kim, Chris Hallacy, Aditya Ramesh, Gabriel Goh, Sandhini Agarwal, Girish Sastry, Amanda Askell, Pamela Mishkin, Jack Clark, et al. Learning transferable visual models from natural language supervision. In *International Conference on Machine Learning*, pages 8748–8763. PMLR, 2021. [2](#)
- [18] Sebastian Ruder. An overview of gradient descent optimization algorithms. *arXiv preprint arXiv:1609.04747*, 2016. [11](#)
- [19] Olga Russakovsky, Jia Deng, Hao Su, Jonathan Krause, Sanjeev Satheesh, Sean Ma, Zhiheng Huang, Andrej Karpathy, Aditya Khosla, Michael Bernstein, et al. Imagenet large scale visual recognition challenge. *International journal of computer vision*, 115(3):211–252, 2015. [6](#)
- [20] Zeyin Song, Yifan Zhao, Yujun Shi, Peixi Peng, Li Yuan, and Yonghong Tian. Learning with fantasy: Semantic-aware virtual contrastive constraint for few-shot class-incremental learning. In *Proceedings of the IEEE/CVF Conference on Computer Vision and Pattern Recognition*, pages 24183–24192, 2023. [12](#), [13](#)
- [21] Yu-Ming Tang, Yi-Xing Peng, and Wei-Shi Zheng. When prompt-based incremental learning does not meet strong pre-training. In *Proceedings of the IEEE/CVF International Conference on Computer Vision*, pages 1706–1716, 2023. [1](#)
- [22] Xiaoyu Tao, Xiaopeng Hong, Xinyuan Chang, Songlin Dong, Xing Wei, and Yihong Gong. Few-shot class-incremental learning. In *Proceedings of the IEEE/CVF Conference on Computer Vision and Pattern Recognition*, pages 12183–12192, 2020. [2](#), [3](#), [12](#), [13](#)
- [23] Oriol Vinyals, Charles Blundell, Timothy Lillicrap, Daan Wierstra, et al. Matching networks for one shot learning. *Advances in neural information processing systems*, 29:3630–3638, 2016. [6](#)

- [24] Catherine Wah, Steve Branson, Peter Welinder, Pietro Perona, and Serge Belongie. The caltech-ucsd birds-200-2011 dataset. 2011. [6](#)
- [25] Runqi Wang, Xiaoyue Duan, Guoliang Kang, Jianzhuang Liu, Shaohui Lin, Songcen Xu, Jinhu Lü, and Baochang Zhang. Attriclip: A non-incremental learner for incremental knowledge learning. In *Proceedings of the IEEE/CVF Conference on Computer Vision and Pattern Recognition*, pages 3654–3663, 2023. [2](#), [3](#), [12](#)
- [26] Shipeng Yan, Jiangwei Xie, and Xuming He. Der: Dynamically expandable representation for class incremental learning. In *Proceedings of the IEEE/CVF Conference on Computer Vision and Pattern Recognition*, pages 3014–3023, 2021. [1](#)
- [27] In-Ug Yoon, Tae-Min Choi, Young-Min Kim, and Jong-Hwan Kim. Balanced supervised contrastive learning for few-shot class-incremental learning. *arXiv preprint arXiv:2305.16687*, 2023. [5](#), [6](#), [7](#), [12](#), [13](#)
- [28] Chi Zhang, Nan Song, Guosheng Lin, Yun Zheng, Pan Pan, and Yinghui Xu. Few-shot incremental learning with continually evolved classifiers. In *Proceedings of the IEEE/CVF Conference on Computer Vision and Pattern Recognition*, pages 12455–12464, 2021. [2](#), [3](#), [7](#), [12](#), [13](#)
- [29] Da-Wei Zhou, Fu-Yun Wang, Han-Jia Ye, Liang Ma, Shiliang Pu, and De-Chuan Zhan. Forward compatible few-shot class-incremental learning. In *Proceedings of the IEEE/CVF Conference on Computer Vision and Pattern Recognition*, pages 9046–9056, 2022. [2](#), [3](#), [5](#), [6](#), [7](#), [12](#), [13](#)
- [30] Da-Wei Zhou, Han-Jia Ye, Liang Ma, Di Xie, Shiliang Pu, and De-Chuan Zhan. Few-shot class-incremental learning by sampling multi-phase tasks. *IEEE Transactions on Pattern Analysis and Machine Intelligence*, 2022. [3](#), [12](#), [13](#)
- [31] Da-Wei Zhou, Yuanhan Zhang, Jingyi Ning, Han-Jia Ye, De-Chuan Zhan, and Ziwei Liu. Learning without forgetting for vision-language models. *arXiv preprint arXiv:2305.19270*, 2023. [3](#)
- [32] Kaiyang Zhou, Jingkang Yang, Chen Change Loy, and Ziwei Liu. Conditional prompt learning for vision-language models. In *Proceedings of the IEEE/CVF Conference on Computer Vision and Pattern Recognition*, pages 16816–16825, 2022. [2](#), [3](#), [6](#), [12](#), [13](#)
- [33] Kaiyang Zhou, Jingkang Yang, Chen Change Loy, and Ziwei Liu. Learning to prompt for vision-language models. *International Journal of Computer Vision*, 130(9):2337–2348, 2022. [3](#), [8](#)
- [34] Yixiong Zou, Shanghang Zhang, Yuhua Li, and Ruixuan Li. Margin-based few-shot class-incremental learning with class-level overfitting mitigation. *arXiv preprint arXiv:2210.04524*, 2022. [12](#), [13](#)

Supplementary Material

A. Further Details

A.1. Implementation Details

We utilized 4 NVIDIA GeForce RTX 3090 GPUs for training and testing. The model was trained by the stochastic gradient descent (SGD) optimizer [18] with a learning rate 0.002, momentum 0.9, and decay 0.0005. The batch size was 16 for both base and incremental sessions. The overall implementation was based on Pytorch.

A.2. Experiment Detail for Fig. 1

We proceeded the FSCIL experiment on the miniImageNet dataset, with ViT-B/16 backbone for the CLIP image encoder. The results are re-implemented values.

A.3. Detailed Structures of the Key-map Network

We mentioned ‘FC1’, ‘FC2’, and the ‘RES2’ options for the key-map network in the Table 3. ‘FC1’ is one fully connected layer with input and output dimension of 512. ‘FC2’ is two fully connected layer with ReLU activation between the layers. ‘RES2’ is two-layer residual layer with structure as linear-ReLU-linear having residual path between the input and the output of second linear layer.

A.4. Implementation Details

We utilized 4 NVIDIA GeForce RTX 3090 GPUs for training and testing. The model was trained by the stochastic gradient descent (SGD) optimizer [18] with a learning rate 0.002, momentum 0.9, and decay 0.0005. The batch size was 16 for both base and incremental sessions. The overall implementation was based on Pytorch.

B. Effects of Randomness During the Key-prompt Initialization

In Section 4.3, we randomly selected indices within the classes of the current session for key-prompt initialization. We utilized five different random seeds and conducted 10 iterations of random key-prompt initialization for each seed. This process was carried out on the miniImageNet dataset, resulting in an average standard deviation of 0.84 for the AVG metric with the mean of 92.2. This relatively low standard deviation helps to support the reliability of our initialization method.

C. Two-dimensional top-K function

Given a two-dimensional function $h(x, y)$ having the integer domains $x \in \{1, \dots, N\}$ and $y \in \{1, \dots, M\}$, we define the two-dimensional $top - K$ function as follows. Firstly,

for integer z , we define quotient and remainder functions as follows:

$$Q(z) = \lfloor (z - 1)/M \rfloor + 1, R(z) = z - (Q(z) - 1)M \quad (15)$$

where $\lfloor \cdot \rfloor$ is a floor function. Then, we define modified a function with single attribute as

$$h^*(z) = h(Q(z), R(z)), \quad (16)$$

for $z \in \{1, \dots, NM\}$. With the function with a single attribute, we obtain $top - K$ index as

$$\{z_l\}_{l=1}^K = \arg \underset{z}{top-K} \{h^*(z)\}_{z=1}^{NM}. \quad (17)$$

Finally, the two-dimensional $top - K$ function is defined as

$$\{Q(z_l), R(z_l)\}_{l=1}^K \equiv \arg \underset{x,y}{top-K} \{\{h(x, y)\}_{y=1}^M\}_{x=1}^N. \quad (18)$$

D. Pseudo-code of proposed algorithm

Pseudo-code of the our overall algorithm is introduced in Algorithm 1.

Algorithm 1 Pseudo-code of overall learning algorithm

Input: Input image dataset $\{\mathcal{D}_{tr}^t, \mathcal{D}_{te}^t\}_{t=1}^T$, CLIP image and text encoder $f_I(\cdot)$ and $f_T(\cdot)$, random initialized key-map $g_\theta(\cdot)$.

Output: Optimized key-map $g_\theta(\cdot)$ and class-wise token embeddings $\{\{E_j^t\}_{j=1}^{m^t}\}_{t=1}^T$ and key-prompt pairs $\{\{k_i^t, Pr_i^t\}_{i=1}^{N^t}\}_{t=1}^T$.

- 1: **for** session $t \in \{1, \dots, T\}$ **do**
 - 2: Initialize class-wise embeddings $\{E_j^t\}_{j=1}^{m^t}$ as Eq. 1
 - 3: Initialize key-prompt pairs $\{k_i^t, Pr_i^t\}_{i=1}^{N^t}$ as Eq. 7
 - 4: Get train data $(x, y) \in \mathcal{D}_{tr}^t$.
 - 5: Get image feature $f(x)$ as Eq. 2.
 - 6: Get key k_x as Eq. 3.
 - 7: Match keys and get index from top-K as Eq. 4.
 - 8: Get prompt bias b_x combining prompts as Eq. 6.
 - 9: Generate classifiers $\{\{g_i^t\}_{i=1}^{m^t}\}_{t'=1}^t$ as Eq. 8.
 - 10: Calculate logits $\{\{p(y_i^{t'}|x)\}_{i=1}^{m^t}\}_{t'=1}^t$ as Eq. 9.
 - 11: Calculate loss function as Eq. 10.
 - 12: Update parameters following Eq. 11.
 - 13: Evaluate the model with \mathcal{D}_{te}^t .
 - 14: **end for**
-

E. Full Comparison Table

In extension to the Table 1, we provide full comparison table including more previous FSCIL methods and the results for PD metric. Results on miniImageNet, CIFAR100, CUB200 datasets are each in Table 6, 7, and 8.

Method	Backbone	Acc. in each session [↑] (%)									AVG([↑])	PD([↓])
		1	2	3	4	5	6	7	8	9		
TOPIC [22]	ResNet18	61.3	50.1	45.2	41.2	37.5	35.5	32.2	29.5	24.4	39.6	36.9
IDLVQ-C [2]	ResNet18	64.8	59.9	55.9	52.6	49.9	47.6	44.8	43.1	41.8	51.2	22.9
CEC [28]	ResNet18	72.0	66.8	63.0	59.4	56.7	53.7	51.2	49.2	47.6	57.7	24.4
Data replay [13]	ResNet18	71.8	67.1	63.2	59.8	57.0	54.0	51.6	49.5	48.2	58.0	23.6
MCNet [9]	ResNet18	72.3	67.7	63.5	60.3	57.6	54.7	52.1	50.4	49.1	58.6	23.3
LIMIT [30]	ResNet18	72.3	68.5	64.3	60.8	58.0	55.1	52.7	50.7	49.2	59.1	23.1
FACT [29]	ResNet18	72.6	69.6	66.4	62.8	60.6	57.3	54.3	52.2	50.5	60.7	22.1
CLOM [34]	ResNet18	73.1	68.1	64.2	60.4	57.4	54.3	51.5	49.4	48.0	58.5	25.1
C-FSCIL [8]	ResNet18	76.4	71.1	66.5	63.3	60.4	57.5	54.8	53.1	51.4	61.6	25.0
ALICE [15]	ResNet18	80.6	70.6	67.4	64.5	62.5	60.0	57.8	56.8	55.7	64.0	24.9
SAVC [20]†	ResNet18	80.5	75.0	72.0	68.0	63.0	62.0	60.0	59.0	58.0	66.4	22.5
BSC [27]	ResNet18	78.4	74.6	71.4	68.7	65.9	63.6	62.0	60.3	58.5	67.1	19.8
ALICE [15]*	ViT-B	88.7	77.3	73.1	71.5	68.9	65.1	62.3	59.9	58.1	69.4	30.6
BSC [27]*	ViT-B	88.2	80.4	76.4	73.2	70.0	67.2	64.5	62.7	61.5	71.6	26.7
CLIP ZSL*	ViT-B/16	85.8	85.5	84.9	84.8	84.2	84.2	84.0	83.9	83.7	84.6	2.1
AttriCLIP [25]	ViT-B/16	90.3	76.4	67.7	60.2	53.9	48.3	44.0	41.1	37.8	57.7	52.5
LGCL [10]	ViT-B/16	95.2	81.6	71.4	63.5	57.4	51.93	47.6	43.94	40.8	61.5	54.4
SV-T [16]	ViT-B/16	90.6	89.2	86.8	85.4	84.8	83.4	81.9	81.9	81.7	85.1	8.9
CoCoOp [32]*	ViT-B/16	94.2	91.7	88.9	87.8	86.3	84.3	82.5	81.9	81.3	86.5	12.9
Ours	ViT-B/16	95.4	94.4	93.4	93.1	92.1	91.4	90.8	90.0	89.1	92.2	6.3

Table 6. Comparison with state-of-the-art methods on the miniImageNet dataset with 5-way 5-shot settings. [↑] means higher is better, while [↓] denotes lower is better. The double horizontal line distinguish whether the CLIP model was used. * mark denotes the re-implemented results, where we re-implemented the CLIP ZSL (zero-shot learning) and CoCoOp for the FSCIL task. Also, we re-implemented ALICE and BSC using ViT-B backbone. The values for SAVC [20]† are estimated values from the figure.

Method	Backbone	Acc. in each session \uparrow (%)									AVG(\uparrow)	PD(\downarrow)
		1	2	3	4	5	6	7	8	9		
TOPIC [22]	ResNet18	64.1	55.9	47.1	45.2	40.1	36.4	34.0	31.6	29.4	42.6	34.7
ERL++ [5]	ResNet18	73.6	68.2	65.1	61.8	58.4	55.5	52.5	50.2	48.2	59.3	25.4
CEC [28]	ResNet18	73.1	68.9	65.3	61.2	58.1	55.6	53.2	51.3	49.1	59.5	23.9
Data replay [13]	ResNet18	74.4	70.2	66.5	62.5	59.7	56.6	54.5	52.4	50.1	60.8	24.3
MCNet [9]	ResNet18	73.3	69.3	65.7	61.7	58.8	56.4	54.6	53.0	50.7	60.4	22.6
LIMIT [30]	ResNet18	73.8	72.1	67.9	63.9	60.7	57.8	55.7	53.5	51.2	61.8	22.6
FACT [29]	ResNet18	74.6	72.1	67.6	63.5	61.4	58.4	56.3	54.2	52.1	62.2	22.5
CLOM [34]	ResNet18	74.2	69.8	66.2	62.4	59.3	56.5	54.4	52.2	50.3	60.6	24.0
C-FSCIL[8]	ResNet18	77.5	72.4	67.5	63.3	59.8	57.0	54.4	52.5	50.5	61.6	27.0
ALICE [15]	ResNet18	79.0	70.5	67.1	63.4	61.2	59.2	58.1	56.3	54.1	63.2	24.9
SAVC [20] \dagger	ResNet18	79.0	73.0	70.0	65.0	62.0	59.0	57.0	55.0	52.0	63.6	27.0
BSC [27]	ResNet18	74.3	70.5	68.5	65.1	62.4	60.4	58.6	56.4	54.7	63.4	19.6
ALICE [15]	ViT-B	85.3	80.7	76.1	71.5	68.1	65.9	62.1	60.1	57.3	69.7	28.0
BSC [27]	ViT-B	85.7	81.5	76.3	72.2	69.4	66.1	64.9	62.5	58.8	70.8	26.9
CLIP ZSL*	ViT-B/16	73.8	71.6	72.0	70.71	69.8	68.5	67.8	67.3	66.9	69.8	6.9
SV-T [16]	ViT-B/16	86.8	82.8	80.4	77.2	76.1	74.0	72.9	71.7	69.8	76.9	17.0
CoCoOp [32]*	ViT-B/16	82.2	77.4	73.7	71.7	69.1	67.7	65.5	63.8	62.1	70.4	20.1
Ours	ViT-B/16	86.2	82.3	79.6	77.5	75.9	75.3	74.1	73.6	72.8	77.5	13.4

Table 7. Comparison with state-of-the-art methods on the CIFAR100 with 5-way 5-shot setting. \uparrow means higher is better, while \downarrow denotes lower is better. The double horizontal line distinguish whether the CLIP model was used. * mark denotes the re-implemented results, where we re-implemented the CLIP ZSL (zero-shot learning) and CoCoOp for the FSCIL task. Also, we re-implemented ALICE and BSC using ViT-B backbone. The values for SAVC [20] \dagger are estimated values from the figure.

Method	Backbone	Acc. in each session \uparrow (%)											AVG(\uparrow)	PD(\downarrow)
		1	2	3	4	5	6	7	8	9	10	11		
TOPIC [22]	ResNet18	68.7	62.5	54.8	50.0	45.3	41.4	38.4	35.4	32.2	28.3	26.3	43.9	42.4
IDLQ-C [2]	ResNet18	77.4	74.7	70.3	67.1	65.3	63.5	62.1	61.5	59.0	58.7	57.8	65.2	19.6
SKD [3]	ResNet18	68.2	60.5	55.7	50.5	45.7	42.9	40.9	38.8	36.5	34.8	33.0	46.1	35.3
ERL++ [5]	ResNet18	73.5	71.1	66.1	63.3	59.5	59.9	58.6	57.7	56.2	54.8	52.3	61.2	21.2
CEC [28]	ResNet18	75.9	71.9	68.5	63.5	62.4	58.3	57.7	55.8	54.8	53.5	52.3	61.3	23.6
Data replay [13]	ResNet18	75.9	72.1	68.6	63.8	62.6	59.1	57.8	55.9	54.9	53.6	52.4	61.5	23.5
MCNet [9]	ResNet18	77.6	74.0	70.5	65.8	66.2	63.8	62.1	61.8	60.4	60.1	59.1	65.6	18.5
LIMIT [30]	ResNet18	75.9	73.6	72.0	68.1	67.4	63.6	62.4	61.4	59.9	58.7	57.4	65.5	18.5
FACT [29]	ResNet18	75.9	73.2	70.8	66.1	65.6	62.2	61.7	59.8	58.4	57.9	56.9	64.4	19.0
CLOM [34]	ResNet18	79.6	76.1	72.9	69.8	67.8	65.6	63.9	62.6	60.6	60.3	59.6	67.2	20.0
ALICE [15]	ResNet18	77.4	72.7	70.6	67.2	65.9	63.4	62.9	61.9	60.5	60.6	60.1	65.7	17.3
SAVC [20] \dagger	ResNet18	81.9	77.9	75.0	70.2	70.0	67.0	66.2	65.3	63.8	63.2	62.5	69.4	19.4
BSC [27]	ResNet18	80.1	76.6	74.0	72.0	70.41	70.3	69.2	66.3	65.6	64.4	63.0	70.2	17.1
CLIP ZSL*	ViT-B/16	65.5	64.2	63.2	62.4	59.9	60.3	59.8	58.4	56.3	54.9	53.5	59.9	12.0
CoCoOp [32]*	ViT-B/16	80.3	72.1	68.8	65.4	63.4	61.2	58.2	56.9	54.5	52.3	50.1	62.1	30.2
Ours	ViT-B/16	81.3	77.4	75.8	73.3	72.6	70.4	68.7	67.3	65.9	64.4	63.8	71.0	17.5

Table 8. Comparison with state-of-the-art methods on the CUB200 dataset with 10-way 5-shot setting. \uparrow means higher is better, while \downarrow denotes lower is better. The double horizontal line distinguish whether the CLIP model was used. * mark denotes the re-implemented results, where we re-implemented the CLIP ZSL (zero-shot learning) and CoCoOp for the FSCIL task. Also, we re-implemented ALICE and BSC using ViT-B backbone. Note that for the CUB200 dataset, the previous methods without using the CLIP model utilize ImageNet-pretrained model.